Thomson scattering system for the diagnosis of the ETE spherical tokamak plasma

L. A. Berni,[a] M. Ueda, E. Del Bosco, J. G. Ferreira, R. M. Oliveira, and W. A. Vilela
Laboratório Associado de Plasma, Instituto Nacional de Pesquisas Espacias (INPE), P.O. Box 515, 12245-970 S.J. Campos, S. Paulo, Brazil

(Received 26 August 2002; accepted 25 November 2002)

A 10 J ruby laser Thomson scattering system was implemented on the ETE spherical tokamak to measure the density n_e and temperature T_e profiles. The laser probes the plasma at the horizontal midplane of the torus and the collection optics allows the observation of up to 22 points inside the plasma in the same plane. Radial profiles of plasma density and electron temperature were obtained for different times during the discharge by shot-to-shot procedure. Temperatures of up to 160 eV and densities of $2.2\times10^{19}\,\mathrm{m}^{-3}$ were measured. Since the level of stray light was too high, the calibration of the Thomson scattering system for density measurements was made using the nitrogen Raman technique instead of the usually applied Rayleigh method.
[DOI: 10.1063/1.1540717]

I. INTRODUCTION

Operation of the ETE spherical tokamak (Experimento Tokamak Esférico) was started at LAP/INPE at the end of 2000. The ETE[1,2] is a small-aspect-ratio device with major radius of 0.3 m and minor radius of 0.2 m. For the first operation stage the following plasma parameters are expected: plasma current up to 220 kA lasting for 15 ms, electron temperature (T_e) of about 300 eV, and electron densities (n_e) in the range of 1×10^{19} to $5\times10^{19}\,\mathrm{m}^{-3}$.

To measure electron temperature and density profiles of the ETE a Thomson scattering (TS) system was implemented. TS is a well-established diagnostic tool for measuring local plasma temperature and density in fusion research experiments with spatial and temporal resolutions.[3–7] This technique is particularly difficult to implement due to the extremely low signals to be detected which can be easily masked by the laser stray light as well as the plasma background radiation. In this work, the main features and the first results of the TS diagnostic of ETE plasma are presented.

II. THOMSON SCATTERING THEORY

The theory of TS is well discussed in a number of texts[8,9] and only a short review relevant to the experiment will be presented here. TS consists basically in the measurement of the scattered light by the electrons of the plasma when irradiated by a high power laser. The measured scattered power in the wavelength range $\Delta\lambda=\lambda_2-\lambda_1$, with the solid angle $\Delta\Omega$, is given by

$$P_s^T = P_i^T \cdot \frac{d\sigma_T}{d\Omega}\cdot n_e \cdot \Delta\Omega \cdot \Delta L \cdot T \cdot G \cdot \eta \times \int_{\lambda_1}^{\lambda_2} S(\lambda,T_e)\cdot\Phi_i(\lambda)\cdot d\lambda, \quad (1)$$

where P_i^T is the incident laser power in the plasma, usually measured by a photodiode, $d\sigma_T/d\Omega$ is the differential Thomson cross section, n_e is the electron density, ΔL is the length of the scattered region as observed by the collection optics, T is the overall transmission of the collection/detection system, G is the gain of the detectors, η is the quantum efficiency of the detectors, $S(\lambda,T_e)$ is the spectral density function where $\int_{-\infty}^{+\infty}S(\lambda,T_e)d\lambda=1$, and $\Phi_i(\lambda)$ is the transfer function of the collection/detection system in the range λ_1 to λ_2. In order to calculate the plasma parameters n_e and T_e it is necessary to know $\Delta\Omega$, ΔL, T, G, η, and $\Phi_i(\lambda)$ to be used in Eq. (1). The transfer function $[\Phi_i(\lambda)]$ is determined using a light source and a calibrated detector. The other parameters can be evaluated by one of the following methods: absolute calibration, Rayleigh scattering, or Raman scattering. In absolute calibration the above parameters can be determined by a standard calibrated light source and by considering the observation geometry. The determination of these individual parameters is a difficult task and large systematic errors can appear, mainly in $\Delta\Omega$ and ΔL evaluation. When performing Raman or Rayleigh scattering all the above parameters are automatically taken into account because these calibration techniques use the same optical setup as TS. Although the Rayleigh scattering calibration technique is usually applied, its use is only recommended for a system presenting a low stray light level, since the scattered light is at the same laser wavelength.[10,11] Raman scattering consists of several lines at both sides of the laser wavelength and for this reason it is noise-free concerning the stray light signals and Mie scattering, but care must be taken in the cross-section evaluation of these lines.[12]

The molecular Raman or Rayleigh scattered power can be expressed as[10]

$$P_s^R = P_i^R \cdot \frac{d\sigma_R}{d\Omega}\cdot n_r \cdot \Delta\Omega \cdot \Delta L \cdot T \cdot G \cdot \eta, \quad (2)$$

where P_i^R is the incident laser power during the calibration,

[a]Electronic mail: berni@plasma.inpe.br

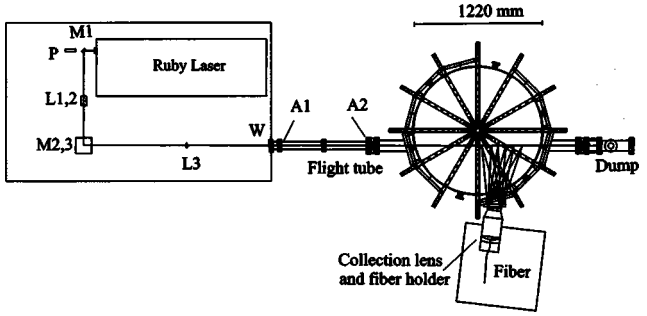

FIG. 1. Thomson scattering on the ETE tokamak. M1,2,3: flat mirrors; P: photodiode; L1,2: beam expander; L3: focusing lens; W: entrance window; and A1,2: apertures.

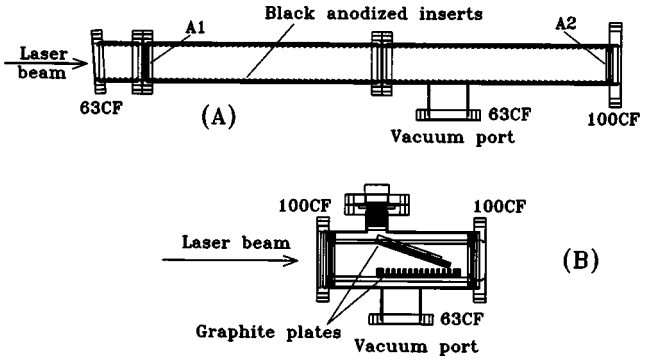

FIG. 2. Schematic diagram of the fight tube (a) and the dump (b).

$d\sigma_R/d\Omega$ is the gas cross section used in the calibration weighted by the detector response at the scattered line, and n_r is the gas density. Using Eqs. (1) and (2) the following expression for the scattered power P^T is obtained:

$$P^T = n_e \cdot \frac{d\sigma_T}{d\Omega} \cdot \frac{d\Omega}{d\sigma_R} \cdot \frac{P^R}{n_r} \cdot \int_{\lambda_1}^{\lambda_2} S(\lambda, T_e) \cdot \Phi_i(\lambda) \cdot d\lambda, \quad (3)$$

where the scattered power in Thomson (P^T) and in Rayleigh or Raman (P^R) was normalized by the incident power P_i^T and P_i^R, respectively. The ratio P^R/n_r is obtained by performing the calibration at several gas pressure values.

The electron temperature can be determined by the ratio of Eq. (3) evaluated for two different spectral channels of the detection system at the same discharge and time. If the temperature is known, the density can be calculated directly from Eq. (3).

III. THOMSON SCATTERING SETUP

Figure 1 shows a schematic diagram of the TS system of the ETE tokamak. A Q-switched ruby laser ($\lambda_r = 6943$ Å) from MBI (series D46550) was chosen as the light source, instead of high repetition rate lasers, since the lifetime of the ETE discharge is planned to be less than 15 ms. The energy of the laser can be scanned from 0.6 to 10 J with 34 ns pulse duration in single mode operation. The laser can also be operated in double pulse mode, with maximum pulse separation of 600 μs with energy of up to 5 J for each pulse. The ruby laser head incorporates an axially aligned HeNe laser that can be used during the alignment procedure.

The injection geometry was designed to allow for full radial coverage on the midplane and to guarantee the probing of the plasma center. The laser beam path is adjusted by three high-energy coated flat mirrors M1, M2, and M3 ($R > 99.5\%$ at 694 nm/45°, damage threshold of 35 J/cm^2), and the plano-convex lens L3 ($f = 3$ m; $R < 0.2\%$ at 694 nm/0°, damage threshold of 15 J/cm^2) focuses the beam in the plasma center. A high-speed photodiode was installed behind mirror M1 for monitoring the laser pulse during the shots. Mirrors M2 and M3 drive the beam in the vertical direction to match with the flight tube apertures as well as to rotate the beam polarization to vertical direction. As this kind of laser usually produces hot points in the beam that can damage any optical component, the beam diameter was expanded from 20 to 30 mm by two standard plano-convex lenses, L1 and L2 (beam expander: $f_1 = -200$ mm and $f_2 = 300$ mm), keeping the energy density well below the threshold limit of the components along the beam path. If necessary, the focusing distance of the injection optics can be adjusted in the range of 2–5 m by changing the separation distance of the lenses in the expander from 104 down to 76 mm, respectively. Presently, the separation distance is fixed at 89 mm assuring a focusing distance of 3 m with a beam diameter of 30 mm at the lens L3.

The laser beam enters the vacuum vessel through a coated 63CF conflat window W ($R < 0.2\%$ at 694 nm/0°, damage threshold of 15 J/cm^2) that is set far from the vessel by a 1.3 m long flight tube. The entrance window is tilted at 4° to avoid any reflection back to the laser head. The flight tube is made of three stainless steel tubes with an internal diameter of 67 mm with its inner surface completely covered by special black anodized aluminum inserts. Two apertures A1 and A2 with a fixed diameter orifice are used to minimize stray light. The aperture A1 ($\phi = 20$ mm) is near the entrance window and the aperture A2 ($\phi = 15$ mm) is placed at the end of the tube. One of the tubes can be connected to a turbomolecular vacuum pump and the other can be removed to decrease the total length. The tube can be isolated from the main vacuum vessel by a manual conflat gate valve. Figure 2(a) shows a schematic drawing with details of the flight tube.

After crossing the vacuum vessel the laser beam is blocked by the dump, which consists of a stainless steel tube with an internal diameter of 98.4 mm with its inner walls black painted with special high temperature ink, and of two graphite plates, one fixed with a special design to minimize stray light (horizontal plate) and one movable that can be adjusted by a vacuum linear motion feed-through to the lowest stray light signal levels, and can be placed out of the path during the alignment procedure. As in the flight tube, the dump can be connected to a vacuum pump and can be separated from the main chamber by a gate valve. Figure 2(b) shows a schematic drawing of the dump.

The scattered light is collected through a 150 CF window ($R < 1\%$ at 660–860 nm/0°), and is imaged by a specially designed $f/6.3$ lens system on a 7 m long fiber bundle (4.5×1.5 mm^2 cross section) with closing packed ends for high efficiency.[13] Figure 3 shows schematically the lens system and gives the characteristics of each lens. Each fiber bundle collects the scattered light by the plasma in a 15 mm

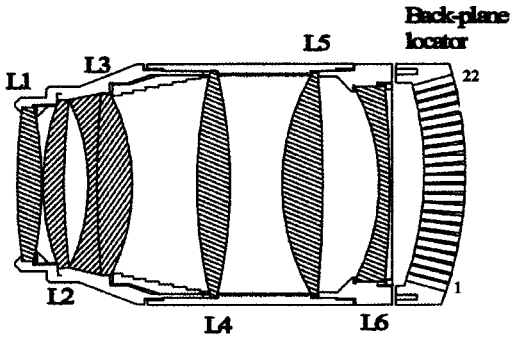

Lens	R1 (mm)	R2 (mm)	R3 (mm)	ϕ (mm)	Thick. (mm)	Glass	Coating
1	429.0	-285.0		112	18	SK5	HEAR1
2	175.0	469.9		122.3	15	SK5	HEAR1
3	-140.5	719.7	-145.9	122.3 132	6 26	SF6 SK5	AR HEAR1
4	350.0	-350.0		165	24	BK7	HEAR1
5	160.0	-848.0		162	30	BK7	HEAR1
6	-145.0	-719.7		142	7.5	SF6	AR

FIG. 3. Schematic diagram of the collection lens and the fiber holder.

region along the beam. During the glow discharge cleaning period, a process for removing the impurities of the inner surface of the vacuum vessel, the window is protected by a specially designed movable screen. The lens system has a back-plane locator (slots) to hold the fiber bundle allowing the light collection from 22 different plasma positions at the same time, covering a total length of 51 cm along the laser beam trajectory. The collected light is analyzed by a five-channel filter polychromator with an avalanche photodiode detector (EG&G C30950E) in each channel optimized for measurements of electron temperatures in the range of 20 eV–2 keV and plasma densities greater than $10^{19}\,\mathrm{m}^{-3}$.[13] Presently, only one polychromator is available so only one plasma position can be measured for each shot. The signals are acquired by a four-channel high speed oscilloscope (Tektronix TDS654C, 5GS/s, 500 MHz).

IV. SYSTEM CALIBRATION AND TEMPERATURE CALCULATION

As mentioned before, in order to determine the plasma parameters the collection/detection system of the TS system must be calibrated. The spectral response of the polychromator was determined by illuminating the fiber bundle end of the collection lens and measuring the signal output of the polychromator. The entrance slit of a $F=640\,\mathrm{mm}$ spectrometer (Jobin Yvon HR640) was uniformily illuminated by a continuous light source with the slits width fixed at 400 μm, resulting in a wavelength band pass of 3.8 Å. The wavelength was scanned between 6900 and 8890 Å by steps of 4 or 10 Å depending on the calibration curve region. The signal at the spectrometer exit slit was measured by the polychromator through the fiber and by a calibrated silicon detector (Oriel model 70286). The ratio of these two signals gives the instrument transfer function as shown in Fig. 4.

Figure 5 shows the present stray light for each channel of the polychromator as a function of the radial position

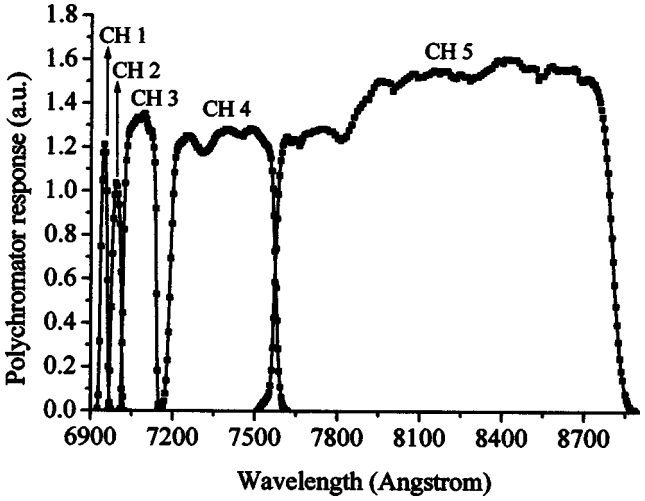

FIG. 4. Spectral calibration of the five channels of the polychromator with the 7 m fiber bundle.

obtained firing the laser with 4.5 J. It can be observed that channel one (for Rayleigh scattering calibration) is completely saturated for all radial positions and for positions in which $r \leqslant 18\,\mathrm{cm}$, the other four channels present a high level of stray light. The high stray light level around the position 16 cm is probably caused by reflections on the inner tube of the toroidal vacuum vessel. Due to the high stray light level, the detection system was calibrated by rotational Raman scattering (stokes lines) with nitrogen gas at pressures between 10 and 100 Torr. The most intense Raman lines were in the range of the second polychromator channel that was used in the calibration. The vacuum vessel was filled with nitrogen at four different pressures values and the scattered signals were measured for each radial position. Figure 6(A) shows the calibration curve for $r=20\,\mathrm{cm}$ and Fig. 6(B) shows the overall calibration curve for 17 radial positions. The Raman signal was normalized by the photodiode signal to compensate for any fluctuation of the laser output energy in each shot. The curve shown in Fig. 6(B) is obtained by

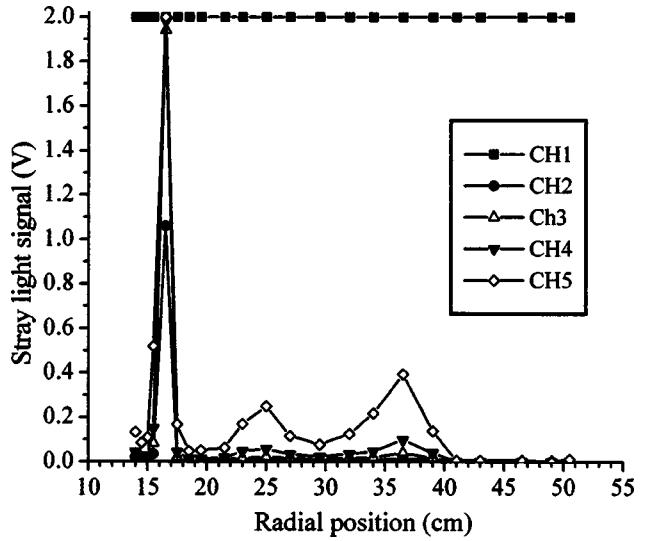

FIG. 5. Stray light profile as a function of the radial position for laser energy of 4.5 J.

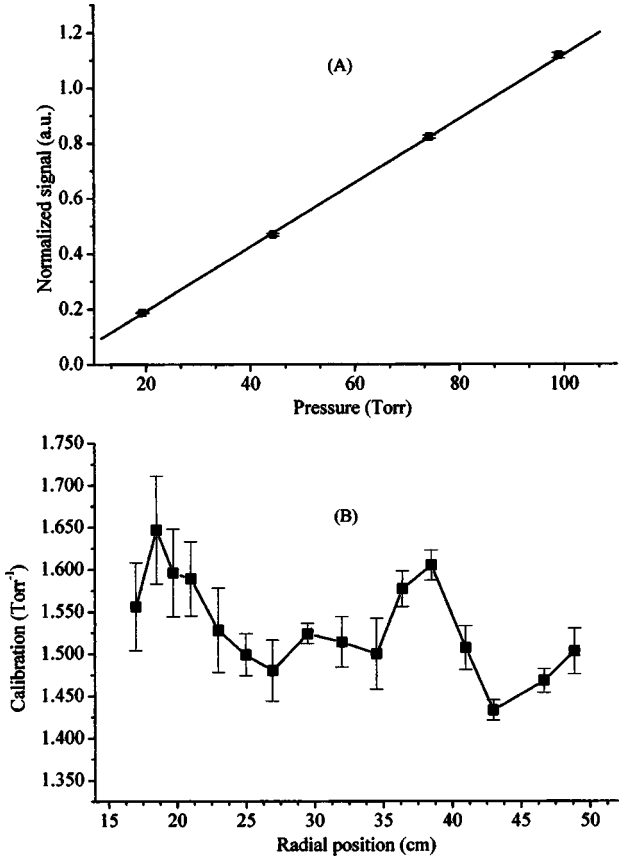

FIG. 6. Raman scattering calibration with nitrogen gas. (A) Normalized scattered signal as a function of the gas pressure for $r=20$ cm (slot 15). (B) Radial profile of the overall calibration.

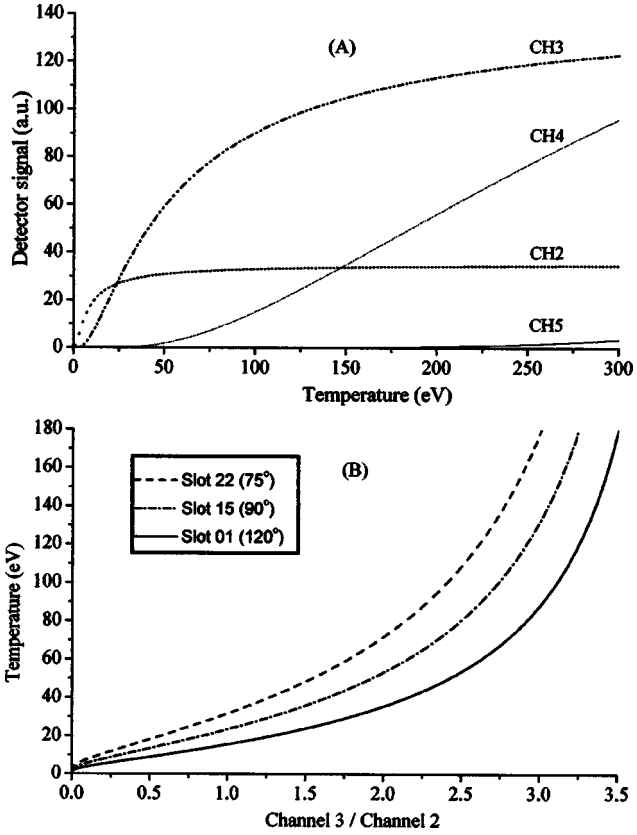

FIG. 7. Temperature evaluation by the ratio of the polychromator channel signals. (A) Channels response for different temperatures for $r=20$ cm (90°). (B) Temperature evaluation by the ratio of channels 2 and 3 for different collecting angles.

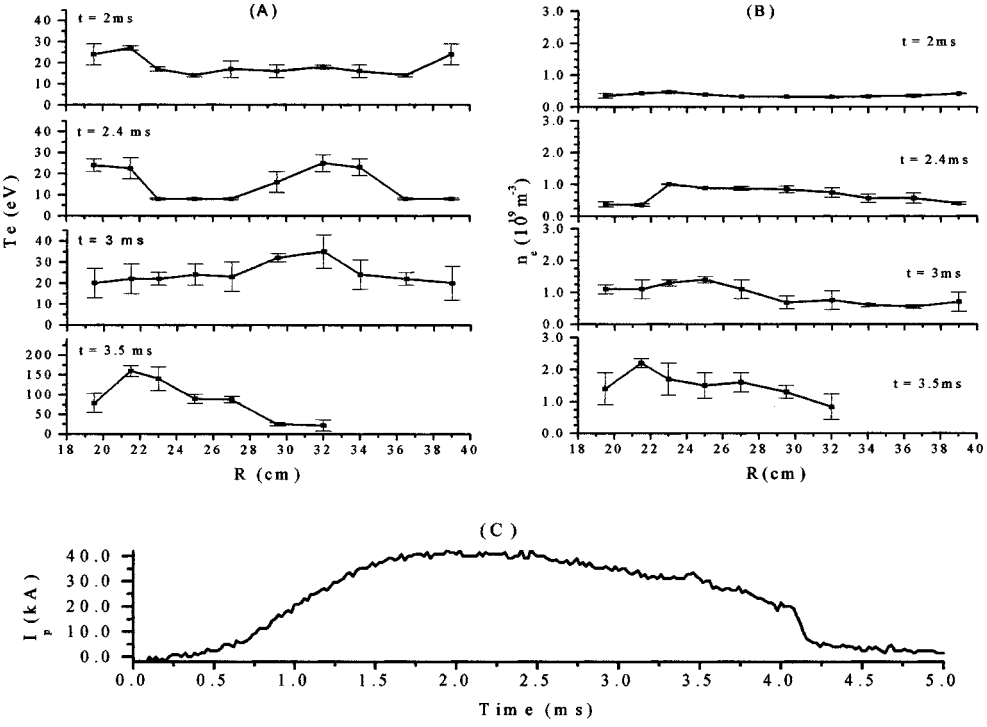

FIG. 8. Radial profile of the temperature (A) and density (B) for a typical ETE shot (C).

calculating the inclination of the best straight line fitted to the measured points for each position, i.e., the P_r/n_r term in Eq. (3).

As mentioned in Sec. II the plasma temperature can be evaluated by the ratio of the signals from the polychromator channels. Figure 7(A) shows the expected signals of channels 2–5 of the polychromator obtained by evaluating Eq. (3) for several temperatures for a scattering angle of 90° (slot $=15$), and taking in account the spectral response of each detector (Fig. 4). Figure 7(B) shows the expected temperature as a function of the ratio of signals from channels 3 and 2 for 90° scattering (slot 15, $r=20\,\mathrm{cm}$) as well as the scattered profile curves for 120° (slot 1, $r=51\,\mathrm{cm}$) and 75° (slot 22, $r=14\,\mathrm{cm}$) scattering angles.

V. RESULTS AND DISCUSSION

The TS system was tested for several different plasma conditions. The temperature and density profiles shown in Fig. 8 were obtained for different times during a typical hydrogen discharge with a plasma current of 40 kA with a duration of 4 ms. Each point in the curves is an average over four shots for each radial position using channels 2 and 3 of the polychromator. The measurement with the other channels was not possible due to the high stray light level. It can be seen from Fig. 8 that both temperature and density increase at the end of the discharge. The T_e varies from nearly 20 eV for $t=2.0\,\mathrm{ms}$ to a peak of 160 eV for $t=3.5\,\mathrm{ms}$ and the density reaches values up to $2.2\times10^{19}\,\mathrm{m}^{-3}$. It can also be verified that the plasma column shifts towards the central tube of the vacuum vessel as the discharge advances in time. This shift is due to the inward force caused by the unbalanced vertical field which for the present coil configuration of ETE is necessary to compensate for the stray fields generated by the induced current in the vacuum vessel during the gas breakdown.

Improvements on the TS optics are in progress mainly to reduce the stray light levels which will allow the measurement with more than two channels, reducing the error in temperature measurement. For the near future more polychromators and a computer automated measurement and control (CAMAC) based acquisition system will be implemented allowing radial temperature/density profiles in a single ETE shot.

ACKNOWLEDGMENTS

The authors would like to acknowledge Dr. Michael Joseph Walsh from Walsh Scientific Ltd. (United Kingdom) for continuous discussion during the TS assembly. This work was partially supported by the Fundaçao de Amparo à Pesquisa do Estado de São Paulo (FAPESP).

[1] E. Del Bosco *et al.*, in Fourteenth IAEA Technical Committee Meeting on Research Using Small Fusion Devices, 2001, Brazil (unpublished).
[2] G. O. Ludwig *et al.*, in Latin American Workshop on Plasma Physics, Argentina, 1998 (unpublished).
[3] D. Dimock *et al.*, Rev. Sci. Instrum. **68**, 700 (1997).
[4] T. N. Caristrom *et al.*, Rev. Sci. Instrum. **63**, 4901 (1992).
[5] M. J. Walsh *et al.*, Rev. Sci. Instrum. **70**, 742 (1999).
[6] M. P. Alonso, P. D. Wilcock, and C. A. F. Varandas, Rev. Sci. Instrum. **70**, 783 (1999).
[7] C. J. Barth, H. J. V. D. Meiden, T. Oyevaar, and N. J. L. Cardozo, Rev. Sci. Instrum. **72**, 1138 (2001).
[8] J. Sheffield, *Plasma Scattering of Electromagnetic Radiation* (Academic, New York, 1975).
[9] A. C. Selden, Phys. Lett. **79A**, 405 (1980).
[10] L. A. Berni *et al.*, Braz. J. Phys. **26**, 755 (1996).
[11] C. J. Barth, C. C. Chu, M. N. A. Beurskens, and H. J. V. D. Meiden, Rev. Sci. Instrum. **72**, 3514 (2001).
[12] J. Howard, B. W. James, and W. I. B. Smith, J. Phys. D **12**, 1435 (1979).
[13] Manufactured by Walsh Scientific Ltd., Culham Science Centre, United Kingdom.